Original Article | Neuroimaging and Head & Neck

eISSN 2005-8330
https://doi.org/10.3348/kjr.2020.0290
Korean J Radiol 2021;22(2):243-252

Korean Journal of Radiology
KJR

Intravoxel Incoherent Motion Magnetic Resonance Imaging for Assessing Parotid Gland Tumors: Correlation and Comparison with Arterial Spin Labeling Imaging

Gao Ma, MS[1]*, Xiao-Quan Xu, PhD[1]*, Liu-Ning Zhu, MD, PhD[2], Jia-Suo Jiang, MS[1], Guo-Yi Su, PhD[1], Hao Hu, PhD[1], Shou-Shan Bu, MD, PhD[2], Fei-Yun Wu, MD, PhD[1]

Departments of [1]Radiology and [2]Stomatology, The First Affiliated Hospital of Nanjing Medical University, Nanjing, China

Objective: To compare and correlate the findings of intravoxel incoherent motion (IVIM) magnetic resonance (MR) imaging and arterial spin labeling (ASL) imaging in characterizing parotid gland tumors.

Materials and Methods: We retrospectively reviewed 56 patients with parotid gland tumors evaluated by MR imaging. The true diffusion coefficient (D), pseudo-diffusion coefficient (D*), and fraction of perfusion (f) values of IVIM imaging and tumor-to-parotid gland signal intensity ratio (SIR) on ASL imaging were calculated. Spearman rank correlation coefficient, chi-squared, Mann-Whitney U, and Kruskal-Wallis tests with the post-hoc Dunn-Bonferroni method and receiver operating characteristic curve assessments were used for statistical analysis.

Results: Malignant parotid gland tumors showed significantly lower D than benign tumors (p = 0.019). Within subgroup analyses, pleomorphic adenomas (PAs) showed significantly higher D than malignant tumors (MTs) and Warthin's tumors (WTs) (p < 0.001). The D* of WTs was significantly higher than that of PAs (p = 0.031). The f and SIR on ASL imaging of WTs were significantly higher than those of MTs and PAs (p < 0.05). Significantly positive correlation was found between SIR on ASL imaging and f (r = 0.446, p = 0.001). In comparison with f, SIR on ASL imaging showed a higher area under curve (0.853 vs. 0.891) in discriminating MTs from WTs, although the difference was not significant (p = 0.720).

Conclusion: IVIM and ASL imaging could help differentiate parotid gland tumors. SIR on ASL imaging showed a significantly positive correlation with f. ASL imaging might hold potential to improve the ability to discriminate MTs from WTs.

Keywords: *Parotid neoplasms; Magnetic resonance imaging; Diffusion magnetic resonance imaging; Perfusion imaging*

INTRODUCTION

Accurate discrimination between benign and malignant parotid gland tumors is important for treatment strategic planning (1). A more aggressive approach, involving total excision of the parotid gland with or without facial nerve removal, is usually applied to treat malignant tumors (MTs). Among benign tumors, since pleomorphic adenomas (PAs) have a higher likelihood of local recurrence, it is also crucial to discriminate PAs from Warthin's tumors (WTs) before surgery. Follow-up can be chosen for WTs, while superficial parotidectomy is the suggested treatment approach for PAs (1, 2). Magnetic resonance (MR) imaging has been widely used for evaluating these tumors (3). However, the efficacy of conventional anatomic imaging is controversial, especially in differentiation between benign and low-grade malignant parotid gland tumors (4).

Recently, several functional MR imaging techniques, which reflect tumor diffusion or perfusion patterns, have been reported to improve the diagnostic accuracy of parotid gland tumors. Diffusion-weighted imaging (DWI), dynamic contrast-enhanced (DCE), and dynamic susceptibility contrast (DSC) perfusion-weighted MR imaging have been frequently used (1, 4-7). However, the apparent diffusion

Received: January 11, 2020 **Revised:** April 14, 2020
Accepted: June 6, 2020
*These authors contributed equally to this work.
Corresponding author: Fei-Yun Wu, MD, PhD, Department of Radiology, The First Affiliated Hospital of Nanjing Medical University, No. 300, Guangzhou Rd., Nanjing 210029, China.
• E-mail: wfy_njmu@163.com

coefficient (ADC) values derived from DWI are also affected by perfusion factors caused by microcapillaries and may limit the reliability of ADC in characterizing parotid gland tumors (8). For DCE and DSC perfusion-weighted imaging, gadolinium-based contrast agents are commonly used, which are invasive and may induce life-threatening adverse reactions for patients with renal dysfunction or allergies to contrast media (9). Furthermore, the complicated quantification of DCE MR imaging parameters limited their widely use in a clinical setting (10).

In contrast, arterial spin labeling (ASL) imaging can quantify tissue perfusion without contrast agents by using magnetically labeled blood water protons as an endogenous tracer (11). ASL imaging showed promising results in assessing the diseased parotid gland with tumors (12, 13) or Sjögren's Syndrome (14). Razek (15) reported that the addition of ASL to DWI imaging could increase the diagnostic accuracy in the differentiation of recurrent head and neck cancer from post-radiation changes. Intravoxel incoherent motion (IVIM) MR imaging is another MR technique that can yield perfusion and diffusion information simultaneously and noninvasively and has attracted increasing attention (16). Previous studies proved the utility of IVIM imaging in parotid gland disorders, such as differentiating benign tumors from MTs, assessing radiation-induced changes, and evaluating organic changes or stages of Sjögren's syndrome (17-20).

Recently, several studies reported that IVIM and ASL imaging had comparable results with DCE imaging for the assessment of tissue perfusion in the head and neck region (21-23). In addition, a few comparative studies were performed to investigate the correlation of perfusion estimation by IVIM and ASL imaging in brain tumors (24-26) and renal allograft function (27). However, comprehensive comparisons and correlations between IVIM and ASL perfusion metrics in parotid gland tumors have not yet been investigated. Therefore, the aims of our study were as follows: first, to assess the diagnostic ability of IVIM and ASL imaging in differentiating parotid benignity from malignancy and second, to evaluate the correlation and comparison of perfusion estimation by IVIM with ASL imaging.

MATERIALS AND METHODS

Study Population

This study was approved by the Institutional Review Board. Requirement of written informed consent was waived due to the retrospective nature of our study. We reviewed the database in our hospital for patients with parotid gland tumors evaluated by MR imaging from January 2017 to May 2018. Fifty-six patients were enrolled in this study on the basis of the following criteria: 1) MR scans were performed before biopsy or treatment; 2) conventional, IVIM and ASL imaging were performed; 3) short-axis diameter of the tumor was greater than 1 cm with sufficient solid areas for placing regions of interest (ROIs); 4) adequate imaging quality for processing; and 5) pathological confirmation after surgery. Among these patients, 44 had benign parotid gland tumors (23 males and 21 females; mean age, 52.7 ± 15.3 years; lesion size, defined as the maximum diameter of tumors measured on axial T2-weighted images, 2.416 ± 0.988 cm) and 12 had MTs (7 males and 5 females; mean age, 48.8 ± 15.6 years; lesion size, 2.816 ± 1.095 cm). The benign tumors included 27 PAs, 13 WTs, and 4 base cell adenomas, while the MTs included three acinic cell carcinomas, two mucosa-associated lymphoid tissue lymphomas, one adenoid cystic carcinoma, one myoepithelial carcinoma, one squamous cell carcinoma, one carcinoma ex PA, one metastatic melanoma, one metastatic squamous cell carcinoma, and one lymphoepithelial carcinoma.

MRI Protocol

All MRI examinations were performed using a 3T MR scanner (MAGNETOM Skyra, Siemens Healthineers) with a 12-channel head and neck coil. Conventional MR images included 1) axial T2-weighted Dixon image with a turbo spin echo (TSE) sequence (repetition time [TR]/echo time [TE], 4000/85 ms; slice number, 25; slice thickness, 4 mm; intersection gap, 20%; field of view [FOV], 200 mm; matrix, 256 x 256); 2) axial T1-weighted image with a TSE sequence (TR/TE, 1460/10 ms; slice number, 40; slice thickness, 4 mm; intersection gap, 10%; FOV, 200 mm; matrix, 320 x 320); and 3) coronal fat-suppressed T2-weighted image with a TSE sequence (TR/TE, 4000/75 ms; slice number, 20; slice thickness, 4 mm; intersection gap, 10%; FOV, 240 mm; matrix, 320 x 320). The total scan time of conventional MRI was about 5 minutes 26 seconds.

IVIM scans were performed with 10 b-values (0, 50, 100, 150, 200, 300, 500, 700, 900, and 1000 s/mm^2) in three orthogonal directions with a readout-segmented echo-planar (RESOLVE) sequence. Other imaging parameters were as follows: TR/TE, 3000/71 ms; slice number, 10; slice

https://doi.org/10.3348/kjr.2020.0290

Korean Journal of Radiology
KJR

thickness, 4 mm; intersection gap, 10%; FOV, 220 mm; matrix, 192 x 192; signal average for each b-value, 1. Total IVIM acquisition time was 6 minutes 53 seconds.

Pulsed ASL imaging with turbo gradient spin echo (TGSE) sequence was performed with the following parameters: TR/TE, 3000/37 ms; inversion time, 1990 ms; bolus duration, 700 ms; slice number, 48; slice thickness, 2 mm; intersection gap, 50%; FOV, 200 mm; matrix, 64 x 64. Total acquisition time of ASL imaging was 3 minutes 18 seconds.

Imaging Analysis

IVIM data were processed with an in-house developed software (FireVoxel, CAI^{2}R) using a bi-exponential IVIM model. ROIs were manually delineated slice-by-slice on IVIM (b_{1000} map) (Fig. 1). The relationship between the signal intensity of IVIM and b-values can be expressed by:

$$S_b/S_0 = (1 - f)\, e^{-bD} + f e^{-bD^*}$$

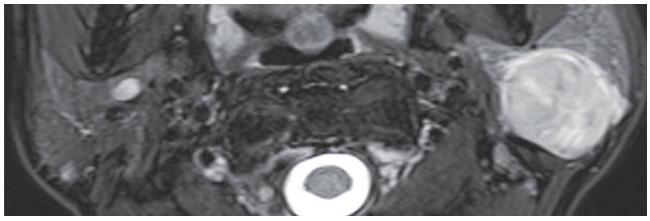

A

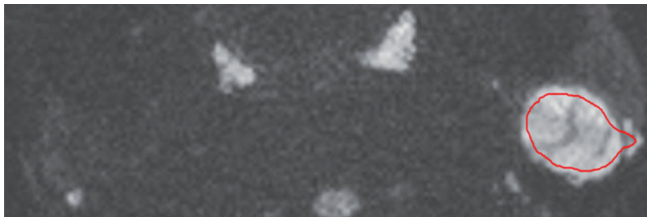

B

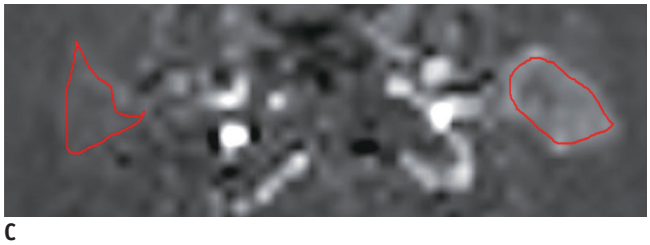

C

Fig. 1. Schematic diagram of ROI placement in a patient with Warthin's tumor.
With reference to the axial TSE-Dixon T2-weighted image **(A)**, irregular ROIs were manually placed to encompass the whole tumor on all slices of the IVIM-b_{1000} map **(B)** in the left gland. Similarly, ROIs were placed to encompass the tumor (left) and contralateral gland (right) on ASL imaging **(C)**. A typical slice is exhibited. ASL = arterial spin labeling, IVIM = intravoxel incoherent motion, ROI = region of interest, TSE = turbo spin echo

where S is signal intensity, b is b-value, f is the fraction of perfusion, D is the true diffusion coefficient, and D* is the pseudo-diffusion coefficient related to perfusion incoherent microcirculation. Data were fitted with the Levenberg-Marquardt nonlinear least squares algorithm. An asymptotic fitting method, which is used to increase the robustness of the fitting with less calculation error, was performed for extracting IVIM parameters with two steps (19, 21). First, the parameter D was calculated with b-values > 200 s/mm^2. Since D* is assumed to be significantly greater than D, the influence of D* on the signal decay at b-values > 200 s/mm^2 can be neglected. Second, keeping D acquired in the first step as a constant value, D* and f can be calculated with all b-values (Fig. 2).

ASL images were transferred into the Siemens workstation (MAGNETOM Skyra) for automated generation of colored perfusion maps. Whole-tumor ROIs were used for ASL intensity measurements on perfusion maps. Mean signal intensity of ASL was calculated with the following equation:

$$ASL = \sum (ASLi \times Si) / \sum Si$$

where ASLi and Si represent the ASL signal intensity and area of the ith slice of parotid gland tumor, respectively. Similarly, the mean signal intensity of the contralateral normal parotid gland was measured, and the tumor-to-parotid gland signal intensity ratio (SIR) was calculated.

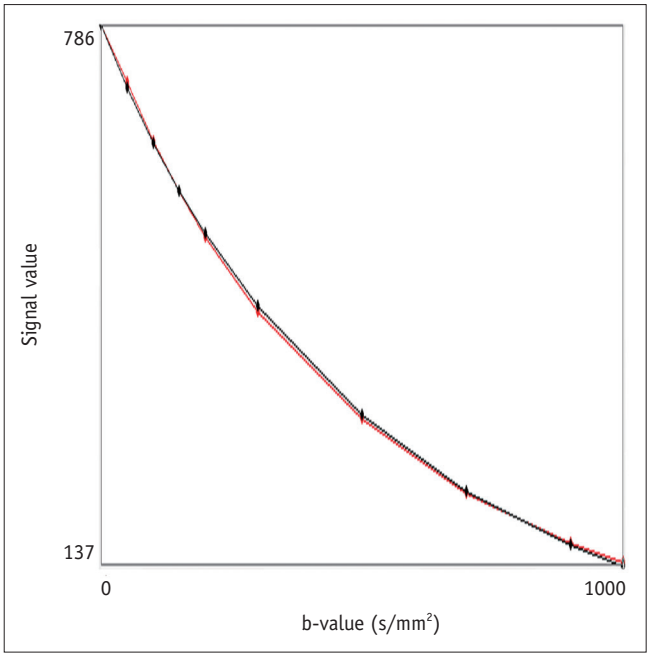

Fig. 2. The IVIM diffusion decay curve (red) and fit curve (black) in a 45-year-old woman with pleomorphic adenoma.

https://doi.org/10.3348/kjr.2020.0290

During placement, the ROI areas were slightly smaller than the actual tumors or normal parotid glands to reduce the influence of the partial volume effect. We excluded obvious vessels and cystic, necrotic, and hemorrhagic components by using T1-weighted and T2-weighted images as reference. If multiple masses occurred, the largest was chosen for analysis. Two head and neck radiologists (reader 1, 4 years of clinical experience; reader 2, 8 years of clinical experience), blind to the study design and pathological diagnosis, individually delineated all the ROIs. The average of the two measurement results was used for further statistical analysis.

Statistical Analysis

All numeric data are reported as mean ± standard deviation. Mann-Whitney U test was used to compare the differences in age, tumor size, IVIM, and ASL parameters between benign and malignant parotid gland tumors, while the chi-squared test was used to compare the differences in gender between the two groups. The correlation of IVIM perfusion-related parameters (f, D*) and SIR on ASL was evaluated by Spearman rank correlation coefficient. Kruskal-Wallis test with the post-hoc Dunn-Bonferroni method was used for comparisons of IVIM and ASL parameters among PAs, WTs, and MTs. Receiver operating characteristic (ROC) curve analyses were used to assess the diagnostic value of significant parameters. Comparisons of ROC curves were performed by the method described by DeLong et al. (28). Intra-class correlation coefficient (ICC) values with 95% confidence interval (CI) were used to evaluate the inter-reader agreement for quantitative measurements. ICC was interpreted as poor when it was < 0.40, moderate if it was 0.41–0.60, good if it was 0.61–0.80, and excellent if it was ≥ 0.81. Statistical analyses were performed using SPSS (Version 23.0, IBM Corp.) and MedCalc (Version 11.0, MedCalc Software bvba). A two-sided *p* value less than 0.05 was considered to indicate statistical significance.

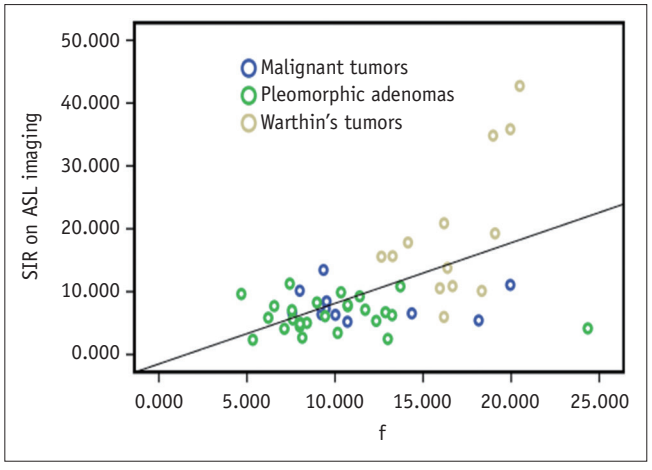

Fig. 3. Scatterplot showing correlation of SIR on ASL imaging with f for malignant tumors, pleomorphic adenomas, and Warthin's tumors. f = fraction of perfusion, SIR = signal intensity ratio

RESULTS

There was no significant difference in age (p = 0.422) and gender distribution (p = 0.755) or tumor size (p = 0.717) between the malignant and benign groups. Significantly positive correlation was observed between SIR on ASL imaging and f (r = 0.446, p = 0.001) (Fig. 3). No significant correlation was found between SIR on ASL imaging and D* (r = 0.216, p = 0.110).

MTs showed significant lower D than the benign tumors (p = 0.019). There was no significant difference in D* (p = 0.826), f (p = 0.549), and SIR on ASL imaging (p = 0.765) between malignant and benign tumors (Table 1). ROC analyses showed that with D ≤ 0.992 x 10^{-3} mm^2/s as the cut-off value, the area under curve (AUC) for differentiating

Table 1. Summary and Comparison of IVIM- and ASL-Derived Parameters

Parameters	Benign Tumors	MTs	PAs	WTs	*P*			
					MTs vs. Benign Tumors	MTs vs. PAs	MTs vs. WTs	PAs vs. WTs
IVIM								
D	1.105 ± 0.403	0.817 ± 0.251	1.338 ± 0.319	0.654 ± 0.122	0.019*	< 0.001*	0.763	< 0.001*
D*	41.165 ± 28.188	47.667 ± 46.805	33.550 ± 22.206	57.988 ± 35.499	0.826	1.000	0.329	0.031*
f	12.049 ± 4.548	11.291 ± 4.013	9.851 ± 3.826	16.787 ± 2.489	0.549	0.896	0.009*	< 0.001*
SIR on ASL	11.298 ± 9.912	7.874 ± 2.494	6.335 ± 2.488	19.527 ± 11.307	0.765	0.489	0.014*	< 0.001*

Data are reported as mean ± standard deviation. The unit of D and D* is x 10^{-3} mm^2/s. *The statistically significant p values. ASL = arterial spin labeling, D = true diffusion coefficient, D* = pseudo-diffusion coefficient, f = fraction of perfusion, IVIM = intravoxel incoherent motion, MT = malignant tumor, PA = pleomorphic adenoma, SIR = signal intensity ratio, WT = Warthin's tumor

https://doi.org/10.3348/kjr.2020.0290

Korean Journal of Radiology
KJR

Table 2. Diagnostic Performance of IVIM- and ASL-Derived Parameters in Discriminating Parotid Gland Tumors

Parameters	Cut-Off Value	Area Under Curve	Sensitivity (100%)	Specificity (100%)
Discriminating MTs from benign tumors				
D	≤ 0.992	0.722	0.833	0.636
Discriminating MTs from PAs				
D	≤ 0.992	0.722	0.833	0.636
Discriminating MTs from WTs				
f	≤ 10.705	0.853	1.000	0.750
SIR on ASL	≤ 13.450	0.891	0.692	1.000
Discriminating PAs from WTs				
D	> 0.912	0.989	1.000	0.926
D*	≤ 38.258	0.758	0.846	0.630
f	≤ 13.240	0.949	0.923	0.926
SIR on ASL	≤ 9.894	0.946	0.923	0.926

The unit of D and D* is x 10^{-3} mm^2/s.

MTs from benign tumors was 0.722, sensitivity was 83.3%, and specificity was 63.6% (Table 2).

MTs had a significantly lower D than PAs ($p < 0.001$), while no significant difference was found in D* ($p = 1.000$), f ($p = 0.896$), and SIR on ASL imaging ($p = 0.489$) between the two groups (Table 1, Fig. 4). With D ≤ 0.992 x 10^{-3} mm^2/s as the cut-off value, the AUC, sensitivity, and specificity for differentiating MTs from PAs were 0.722, 83.3%, and 63.6%, respectively (Table 2).

There was no significant difference in D ($p = 0.763$) and D* ($p = 0.329$) between MTs and WTs, while MTs showed significantly lower f ($p = 0.009$) and SIR on ASL imaging ($p = 0.014$) than WTs (Table 1, Fig. 4). SIR on ASL imaging showed a higher AUC than f in discriminating between MTs and WTs, although the difference did not reach significance (AUC, 0.891 vs. 0.853; sensitivity, 69.2% vs. 100%; specificity, 100% vs. 75.0%; $p = 0.720$) (Table 2, Fig. 5).

PAs showed significantly higher D ($p < 0.001$) and lower D* ($p = 0.031$), f ($p < 0.001$), and SIR on ASL imaging ($p < 0.001$) than WTs (Table 1, Fig. 4). D (cut-off value, > 0.912 x 10^{-3} mm^2/s; AUC, 0.989; sensitivity, 100%; specificity, 92.6%) demonstrated optimal performance that was significantly better than that of D* ($p = 0.005$), although the difference in AUC between D and f ($p = 0.335$) or SIR on ASL imaging ($p = 0.334$) did not reach significance (Table 2, Fig. 5). Representative images of acinic cell carcinoma, PA, and WT are shown in Figure 6.

Good to excellent inter-reader agreements were achieved for quantitative measurements of D (ICC [95% CI], 0.839 [0.726–0.906]), D* (0.757 [0.586–0.858]), f (0.905 [0.838–0.944]), and SIR on ASL imaging (0.907 [0.842–0.946]).

DISCUSSION

Our study found that IVIM imaging-related parameters could be useful for differentiating malignant and benign parotid gland tumors. Within subgroup analyses, IVIM imaging demonstrated the distinctive parameters of MTs, PAs, and WTs. SIR on ASL imaging was significantly positively correlated with f. ASL imaging could also help differentiate WTs from MTs and PAs. In comparison with f, SIR on ASL imaging might hold potential to improve the ability to discriminate MTs from WTs. To the best of our knowledge, our study is the first to compare and correlate the findings of the two different non-contrast-enhanced perfusion techniques in characterizing parotid gland tumors.

Similar to previous DWI studies (7), malignant parotid gland tumors showed significantly lower D than benign tumors. Within subgroup analyses, consistent with the previous study (13), PAs showed significantly higher D than MTs and WTs, while there was an overlap in D between MTs and WTs. However, f showed compensatory efficiency in differentiating MTs from WTs, and f of WTs was significantly higher than those of MTs and PAs. Similarly, Dong et al. (29) reported that the blood flow in CT perfusion imaging for WTs was significantly higher. On the other hand, although Sumi et al. (17) also reported higher f in WTs than in MTs, the difference did not reach significance. This discrepancy might be attributed to the different histopathological subtypes of MTs and the differences in IVIM imaging parameters between the two studies. Since f was dependent on the fractional volume of capillary blood flowing in each voxel and reflected intact vascular permeability (10), we

 https://doi.org/10.3348/kjr.2020.0290

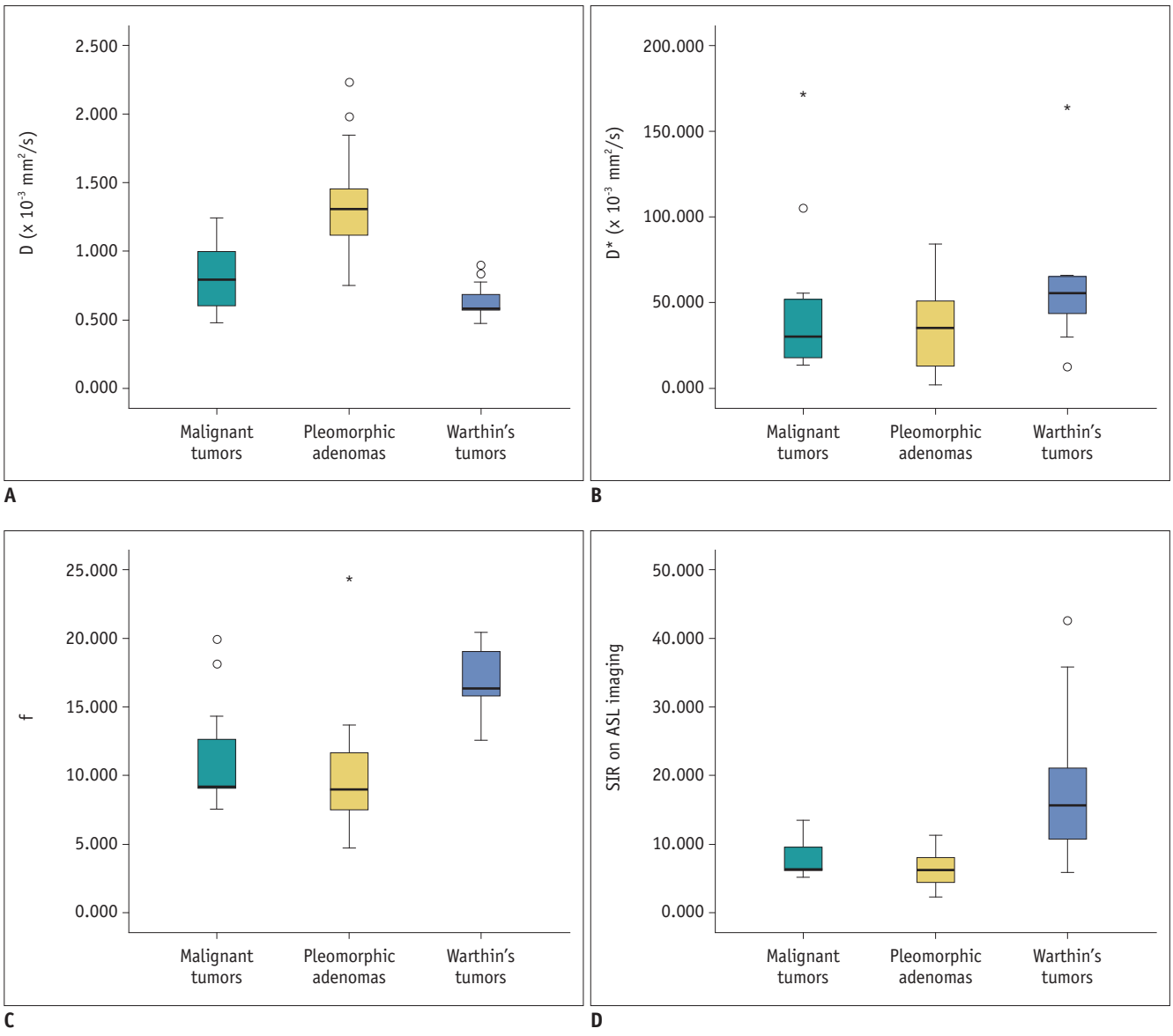

Fig. 4. Box plots showing comparison of D (A), D*(B), f (C), and SIR values on ASL imaging (D) among malignant tumors, pleomorphic adenomas, and Warthin's tumors. The line in the box represents the median. The height of the box represents the interquartile range. Whiskers are lowest and highest data points within a 1.5 interquartile range. Circles and asterisks indicate outliers. D = true diffusion coefficient, D* = pseudo-diffusion coefficient

could deduce that WTs may have a higher capillary density (16, 29).

We found a significantly positive correlation between SIR on ASL imaging and f. Dolgorsuren et al. (24) reported the correlation between ASL-derived cerebral blood flow and f in brain tumors, and the correlation coefficient was 0.414, which corresponded well with our result. No significant correlation was found between SIR on ASL imaging and D* in our study. The reason might be that D* was considered to contain more information on permeability due to pathological changes in tumors than f, which cannot be obtained with ASL perfusion data (24, 25).

In agreement with previous studies (12, 13), SIR on ASL imaging could also differentiate WTs from the other two pathologies. Furthermore, SIR on ASL imaging showed higher AUCs than f in discriminating MTs from WTs, although the difference did not reach significance. This might have occurred because ASL imaging could directly determine the intravascular blood volume not affected by vessel permeability. Thus, estimation of the micro-perfusion effect by ASL imaging might be more accurate than that with f, leading to a higher specificity (14). Previously,

https://doi.org/10.3348/kjr.2020.0290

Korean Journal of Radiology
KJR

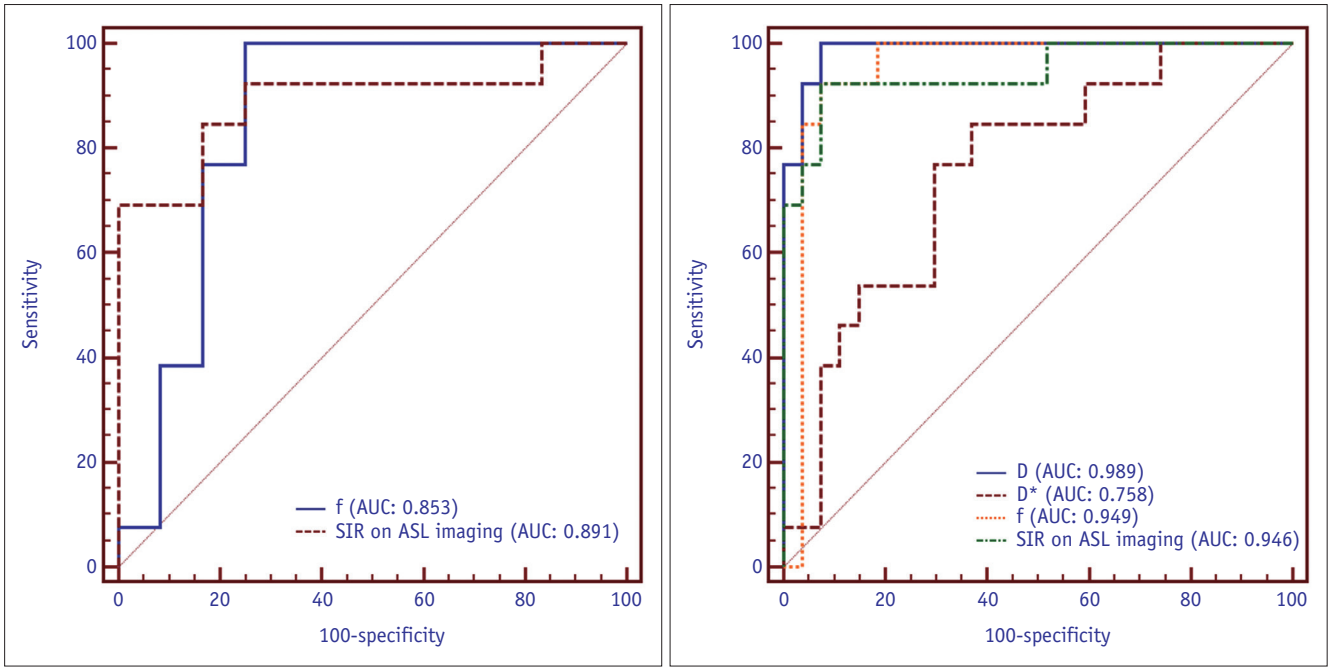

A B

Fig. 5. Comparison of the diagnostic ability of different parameters for discriminating Warthin's tumor from malignant tumors (A) or pleomorphic adenomas (B). AUC = area under curve

Yamamoto et al. (23) found that the microvessel density of WTs was significantly higher than that of PAs histologically, and tumor blood flow evaluated by ASL imaging had a positive correlation with the number of microvessels. Further studies that correlate the histological examination with parameters derived from IVIM or ASL imaging might be helpful to fully understand the relationship among these parameters.

DCE perfusion techniques also showed high value for differential diagnosis in head and neck tumors when semi-quantitatively used with time-intensity curve patterns or quantitatively used with perfusion-related parameters such as k-trans, plasma volume, and the volume of extracellular space (30). However, DCE MR imaging is more difficult to implement into routine clinical protocols because of the limited reliability of the arterial input function and the large number of potential perfusion-related parameters for investigation (10). In contrast, IVIM and ASL imaging can be performed safely and repeatedly because of its noninvasiveness (11, 16). Moreover, Fujima et al. (31) found that tumor blood flow measured by ASL imaging might be more accurate than DCE MR imaging. However, the interpretation was still controversial due to the influence of cardiac cycle for IVIM and the low signal intensity-to-noise ratio for ASL imaging (32, 33). In our study, RESOLVE and three-dimensional TGSE sequences were used for IVIM and ASL imaging respectively, which proved effective in significantly improving image quality (33, 34).

Besides the small cohort, our study also has several limitations. First, there were various histological subtypes in malignant parotid gland tumors and the sample size for each type was small; therefore, some crucial subgroup differentiations among MTs could not to be performed. Furthermore, the majority of MTs in our study were acinic cell carcinomas and lymphomas characterized by low ADC values and could affect the interpretation of the results. However, we believe that further studies with large cohorts could help clarify the value of IVIM and ASL imaging in such subgroup differentiations and confirm the findings of our study. Second, the specific b-value range used for the RESOLVE sequence in our study was chosen in the order recommended by Lemke et al. (35), with at least 10 b-values, of which many were concentrated in the low range (< 200 s/mm^2). However, only 5 b-values at an interval of 50 s/mm^2 (0, 50, 100, 150, and 200 s/mm^2) in the low range were used in our study due to the limitations of the MR scanning system, which might have slightly affected the quantification of IVIM parameters. A greater number of b-values less than 200 s/mm^2 would be better at showing the perfusion features of IVIM imaging for parotid gland tumors. Third, quantification of the goodness of the IVIM fits, which is important for assessment of the reliability

 https://doi.org/10.3348/kjr.2020.0290

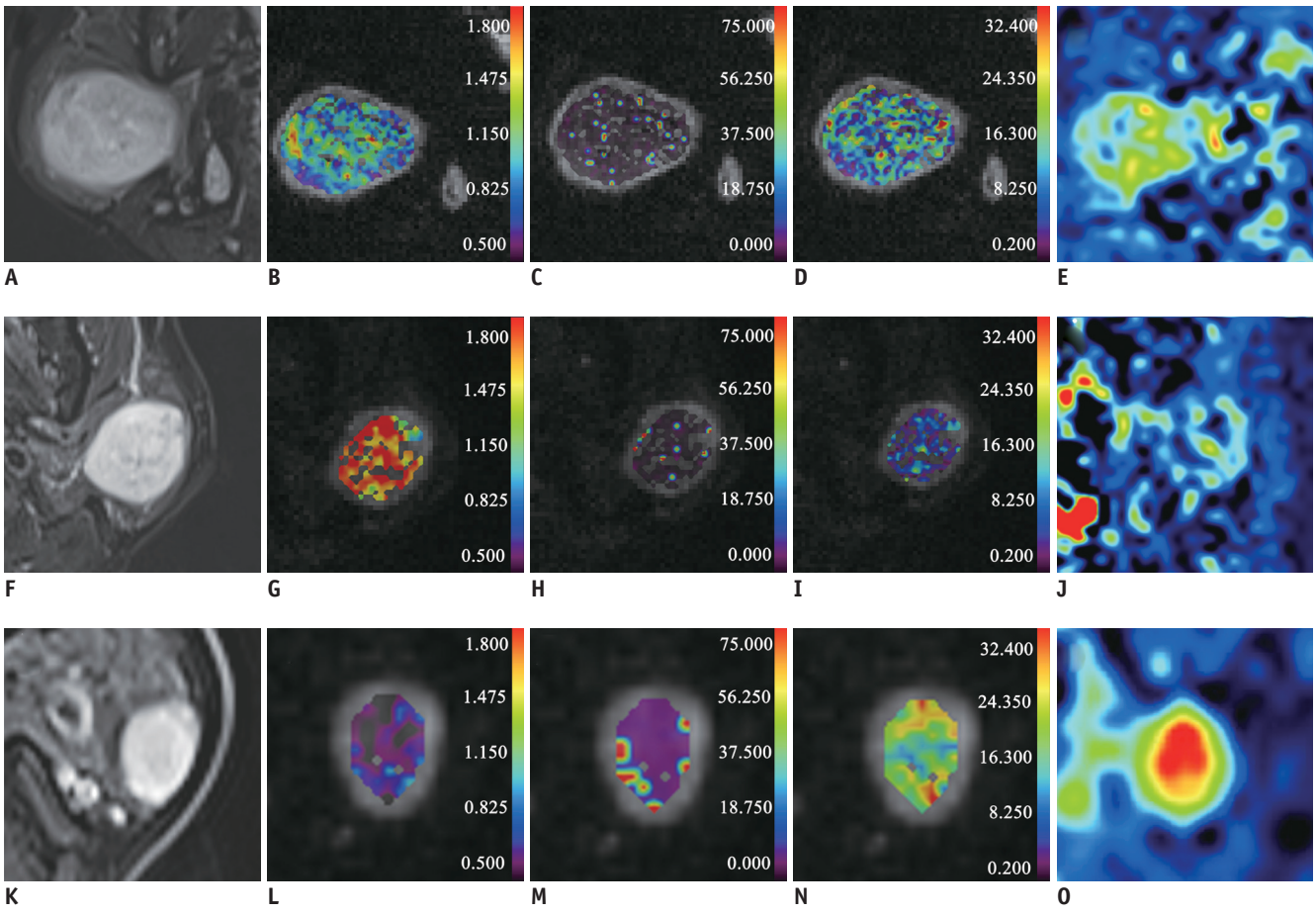

Fig. 6. Representative images of acinic cell carcinoma (A-E), pleomorphic adenoma (F-J), and Warthin's tumor (K-O). The left column was the axial TSE-Dixon T2-weighted image **(A, F, K)**. The following columns were colored D **(B, G, L)**, D* **(C, H, M)**, and f **(D, I, N)** maps embedded into the diffusion images (b_{1000} map) and ASL **(E, J, O)** maps. Corresponding maps showed a relatively higher D **(G)**, lower D* **(H)**, f **(I)**, and ASL intensity **(J)** of pleomorphic adenoma than that of acinic cell carcinoma **(B-E)** and Warthin's tumor **(L-O)**. The unit of D and D* is x 10^{-3} mm^2/s.

of the measurement of IVIM parameters (36), was not conducted. Further analyses are required to solve this question. Fourth, we did not include the imaging features on conventional MR imaging into statistical analysis. Further studies combining conventional and functional MR imaging might yield more accurate diagnostic performance. Fifth, the ROIs of the tumors were not the same between IVIM and ASL imaging, so we used whole-tumor ROIs to ensure higher reproducibility. However, this approach was time-consuming, and future studies using computer-aided imaging analysis might be more valuable.

In conclusion, our study showed that IVIM and ASL imaging could help to differentiate parotid gland tumors. SIR on ASL imaging showed a significantly positive correlation with f. ASL imaging might have the potential to improve the diagnostic ability in differentiating WTs from MTs.

Conflicts of Interest

The authors have no potential conflicts of interest to disclose.

ORCID iDs

Gao Ma
https://orcid.org/0000-0002-9333-9227
Xiao-Quan Xu
https://orcid.org/0000-0001-5493-5256
Liu-Ning Zhu
https://orcid.org/0000-0001-7117-5893
Jia-Suo Jiang
https://orcid.org/0000-0001-9404-4829
Guo-Yi Su
https://orcid.org/0000-0002-1826-3234
Hao Hu
https://orcid.org/0000-0002-7983-7377

https://doi.org/10.3348/kjr.2020.0290

Korean Journal of Radiology
KJR

Shou-Shan Bu
https://orcid.org/0000-0002-7735-7011
Fei-Yun Wu
https://orcid.org/0000-0002-3479-369X

REFERENCES

1. Gökçe E. Multiparametric magnetic resonance imaging for the diagnosis and differential diagnosis of parotid gland tumors. *J Magn Reson Imaging* 2020;52:11-32
2. Razek AAKA. Characterization of salivary gland tumours with diffusion tensor imaging. *Dentomaxillofac Radiol* 2018;47:20170343
3. Razek AAKA, Mukherji SK. State-of-the-art imaging of salivary gland tumors. *Neuroimaging Clin N Am* 2018;28:303-317
4. Razek AAKA. Routine and advanced diffusion imaging modules of the salivary glands. *Neuroimaging Clin N Am* 2018;28:245-254
5. Eida S, Sumi M, Nakamura T. Multiparametric magnetic resonance imaging for the differentiation between benign and malignant salivary gland tumors. *J Magn Reson Imaging* 2010;31:673-679
6. Tao X, Yang G, Wang P, Wu Y, Zhu W, Shi H, et al. The value of combining conventional, diffusion-weighted and dynamic contrast-enhanced MR imaging for the diagnosis of parotid gland tumours. *Dentomaxillofac Radiol* 2017;46:20160434
7. Razek AAKA, Samir S, Ashmalla GA. Characterization of parotid tumors with dynamic susceptibility contrast perfusion-weighted magnetic resonance imaging and diffusion-weighted MR imaging. *J Comput Assist Tomogr* 2017;41:131-136
8. Sakamoto J, Imaizumi A, Sasaki Y, Kamio T, Wakoh M, Otonari-Yamamoto M, et al. Comparison of accuracy of intravoxel incoherent motion and apparent diffusion coefficient techniques for predicting malignancy of head and neck tumors using half-Fourier single-shot turbo spin-echo diffusion-weighted imaging. *Magn Reson Imaging* 2014;32:860-866
9. Choi JW, Moon WJ. Gadolinium deposition in the brain: current updates. *Korean J Radiol* 2019;20:134-147
10. Dai YL, King AD. State of the art MRI in head and neck cancer. *Clin Radiol* 2018;73:45-59
11. Alsop DC, Detre JA. Multisection cerebral blood flow MR imaging with continuous arterial spin labeling. *Radiology* 1998;208:410-416
12. Kato H, Kanematsu M, Watanabe H, Kajita K, Mizuta K, Aoki M, et al. Perfusion imaging of parotid gland tumours: usefulness of arterial spin labeling for differentiating Warthin's tumours. *Eur Radiol* 2015;25:3247-3254
13. Razek AAKA. Multi-parametric MR imaging using pseudo-continuous arterial-spin labeling and diffusion-weighted MR imaging in differentiating subtypes of parotid tumors. *Magn Reson Imaging* 2019;63:55-59
14. Kami YN, Sumi M, Takagi Y, Sasaki M, Uetani M, Nakamura T. Arterial spin labeling imaging for the parotid glands of patients with Sjögren's syndrome. *PLoS One* 2016;11:e0150680
15. Razek AAKA. Arterial spin labelling and diffusion-weighted magnetic resonance imaging in differentiation of recurrent head and neck cancer from post-radiation changes. *J Laryngol Otol* 2018;132:923-928
16. Le Bihan D, Breton E, Lallemand D, Aubin ML, Vignaud J, Laval-Jeantet M. Separation of diffusion and perfusion in intravoxel incoherent motion MR imaging. *Radiology* 1988;168:497-505
17. Sumi M, Van Cauteren M, Sumi T, Obara M, Ichikawa Y, Nakamura T. Salivary gland tumors: use of intravoxel incoherent motion MR imaging for assessment of diffusion and perfusion for the differentiation of benign from malignant tumors. *Radiology* 2012;263:770-777
18. Shen J, Xu XQ, Su GY, Hu H, Shi HB, Liu W, et al. Intravoxel incoherent motion magnetic resonance imaging of the normal-appearing parotid glands in patients with differentiated thyroid cancer after radioiodine therapy. *Acta Radiol* 2018;59:204-211
19. Su GY, Xu XQ, Wang YY, Hu H, Shen J, Hong XN, et al. Feasibility study of using intravoxel incoherent motion MRI to detect parotid gland abnormalities in early-stage Sjögren syndrome patients. *J Magn Reson Imaging* 2016;43:1455-1461
20. Chu C, Zhou N, Zhang H, Dou X, Li M, Liu S, et al. Correlation between intravoxel incoherent motion MR parameters and MR nodular grade of parotid glands in patients with Sjögren's syndrome: a pilot study. *Eur J Radiol* 2017;86:241-247
21. Fujima N, Yoshida D, Sakashita T, Homma A, Tsukahara A, Tha KK, et al. Intravoxel incoherent motion diffusion-weighted imaging in head and neck squamous cell carcinoma: assessment of perfusion-related parameters compared to dynamic contrast-enhanced MRI. *Magn Reson Imaging* 2014;32:1206-1213
22. Lin M, Yu X, Luo D, Ouyang H, Xie L, Wu B, et al. Investigating the correlation of arterial spin labeling and dynamic contrast enhanced perfusion in primary tumor of nasopharyngeal carcinoma. *Eur J Radiol* 2018;108:222-229
23. Yamamoto T, Kimura H, Hayashi K, Imamura Y, Mori M. Pseudo-continuous arterial spin labeling MR images in Warthin tumors and pleomorphic adenomas of the parotid gland: qualitative and quantitative analyses and their correlation with histopathologic and DWI and dynamic contrast enhanced MRI findings. *Neuroradiology* 2018;60:803-812
24. Dolgorsuren EA, Harada M, Kanazawa Y, Abe T, Otomo M, Matsumoto Y, et al. Correlation and characteristics of intravoxel incoherent motion and arterial spin labeling techniques versus multiple parameters obtained on dynamic susceptibility contrast perfusion MRI for brain tumors. *J Med Invest* 2019;66:308-313
25. Shen N, Zhao L, Jiang J, Jiang R, Su C, Zhang S, et al. Intravoxel incoherent motion diffusion-weighted imaging analysis of diffusion and microperfusion in grading gliomas and comparison with arterial spin labeling for evaluation of tumor perfusion. *J Magn Reson Imaging* 2016;44:620-632

 https://doi.org/10.3348/kjr.2020.0290

26. Lin Y, Li J, Zhang Z, Xu Q, Zhou Z, Zhang Z, et al. Comparison of intravoxel incoherent motion diffusion-weighted MR imaging and arterial spin labeling MR imaging in gliomas. *Biomed Res Int* 2015;2015:234245
27. Ren T, Wen CL, Chen LH, Xie SS, Cheng Y, Fu YX, et al. Evaluation of renal allografts function early after transplantation using intravoxel incoherent motion and arterial spin labeling MRI. *Magn Reson Imaging* 2016;34:908-914
28. DeLong ER, DeLong DM, Clarke-Pearson DL. Comparing the areas under two or more correlated receiver operating characteristic curves: a nonparametric approach. *Biometrics* 1988;44:837-845
29. Dong Y, Lei GW, Wang SW, Zheng SW, Ge Y, Wei FC. Diagnostic value of CT perfusion imaging for parotid neoplasms. *Dentomaxillofac Radiol* 2014;43:20130237
30. Lee FK, King AD, Ma BB, Yeung DK. Dynamic contrast enhancement magnetic resonance imaging (DCE-MRI) for differential diagnosis in head and neck cancers. *Eur J Radiol* 2012;81:784-788
31. Fujima N, Kudo K, Tsukahara A, Yoshida D, Sakashita T, Homma A, et al. Measurement of tumor blood flow in head and neck squamous cell carcinoma by pseudo-continuous arterial spin labeling: comparison with dynamic contrast-enhanced MRI. *J Magn Reson Imaging* 2015;41:983-991
32. Federau C, Hagmann P, Maeder P, Müller M, Meuli R, Stuber M, et al. Dependence of brain intravoxel incoherent motion perfusion parameters on the cardiac cycle. *PLoS One* 2013;8:e72856
33. Günther M, Oshio K, Feinberg DA. Single-shot 3D imaging techniques improve arterial spin labeling perfusion measurements. *Magn Reson Med* 2005;54:491-498
34. Bogner W, Pinker-Domenig K, Bickel H, Chmelik M, Weber M, Helbich TH, et al. Readout-segmented echo-planar imaging improves the diagnostic performance of diffusion-weighted MR breast examinations at 3.0 T. *Radiology* 2012;263:64-76
35. Lemke A, Stieltjes B, Schad LR, Laun FB. Toward an optimal distribution of b values for intravoxel incoherent motion imaging. *Magn Reson Imaging* 2011;29:766-776
36. Yuan J, Wong OL, Lo GG, Chan HHL, Wong TT, Cheung PSY. Statistical assessment of bi-exponential diffusion weighted imaging signal characteristics induced by intravoxel incoherent motion in malignant breast tumors. *Quant Imaging Med Surg* 2016;6:418-429

https://doi.org/10.3348/kjr.2020.0290